Hybrid Beamforming for Wideband Millimeter Wave MIMO Integrated Sensing and Communications

Junpeng Guo, *Student Member, IEEE* and Chenhao Qi, *Senior Member, IEEE*

***Abstract*—In this letter, we propose a true-time-delayer network assisted hybrid beamforming scheme for wideband millimeter wave multiple-input multiple-output integrated sensing and communications. By jointly optimizing the digital beamformer, the true-time-delayer network and the phase shifter network, we aim at making the sum of beam patterns across all subcarriers approach a predefined sensing beam pattern, subject to the constraints of the signal-to-interference-plus-noise ratio requirements of communication users and the maximum transmit power of the base station. To improve the design flexibility, the sensing beam pattern is distributed among different subcarriers for optimization, with phase vectors introduced to transform the modulus summation into a linear summation. Additionally, by decoupling the multi-variable constraint, we employ the alternating direction method of multipliers to decompose the original problem into manageable subproblems, which are iteratively optimized. Simulation results demonstrate that the proposed scheme outperforms existing hybrid beamforming schemes in terms of beam pattern and sensing performance.**

***Index Terms*—Alternating direction method of multipliers, integrated sensing and communications, second-order cone programming, wideband hybrid beamforming.**

I. Introduction

With the development of information technology, the requirements for communication quality are increasing, necessitating high transmission rates, low service latency and strong system robustness. Consequently, the standardization of 6G wireless networks has become a priority. Among the new application scenarios, integrated sensing and communications (ISAC) have attracted widespread attention from academia and industry. By utilizing the similarities between communication and sensing signals, the system can simultaneously serve for the communication and sensing purposes.

The ISAC systems typically use orthogonal frequency division multiplexing (OFDM) modulation and multiple-input multiple-output (MIMO) technologies to achieve joint allocation of frequency and spatial resources. In [1], a two-step hybrid beamforming scheme in MIMO ISAC system considering the signal-to-interference-plus-noise ratio (SINR) constraint for communication users is proposed, where the fully digital beamformer is obtained at first and then the hybrid beamformer is determined. As system bandwidth increases, in-depth studies of wideband MIMO systems become increasingly significant. Wideband systems may cause angle modulation effects in analog beamforming, leading to severe performance degradation in massive MIMO systems. To combat these effects, deliberately designed compensation can be performed for digital beamforming according to the severity of the beam squint [2]. To mitigate angle modulation effects from system level, a true-time-delayer (TTD) based delay-phase precoding architecture is proposed, generating a frequency-dependent beamforming architecture to improve over the conventional frequency-independent analog beamforming [3]. Beam squint effects have also been studied in ISAC systems. By leveraging beam squint effects, narrow beams at different frequencies are superimposed into a wide beam for user position sensing, and then the angle modulation effect is eliminated during the communication phase [4]. The existing literature focuses on eliminating the squint effect of a single beam, and it would be interesting to investigate how to achieve multi-beam alignment simultaneously.

In this letter, we propose a true-time-delayer (TTD) network assisted hybrid beamforming (TTDHBF) scheme for wideband millimeter wave (mmWave) MIMO ISAC system. By jointly optimizing the digital beamformer, the TTD network and the phase shifter network, we aim at making the sum of beam patterns across all subcarriers approach a predefined sensing beam pattern, subject to the constraints of the SINR requirements of the communications users and the maximum transmit power of the base station (BS). To improve the design flexibility, the sensing beam pattern is distributed among different subcarriers for optimization, with phase vectors introduced to transform the modulus summation into a linear summation. Additionally, by decoupling the multi-variable constraint, we employ the alternating direction method of multipliers (ADMM) to decompose the problem into manageable subproblems, which are iteratively optimized.

Notations: Symbols for matrices and vectors are denoted in boldface. $(\,)^{\mathrm{T}}$, $(\,)^{\mathrm{H}}$, $(\,)^{-1}$, $(\,)^{\dagger}$, $\|\,\|_2$, $\|\,\|_{\mathrm{F}}$, $|\,|$, $\angle$ and $\mathbb{E}\{\,\}$ denote the transpose, the conjugate transpose, the inverse, the pseudo-inverse, the ℓ_2 norm, the Frobenius norm, the modulus, the phase and the expectation, respectively. $[\boldsymbol{a}]_m$ represents the mth entry of a vector $\boldsymbol{a}$. $\boldsymbol{I}_K$ denotes a K-by-K identity matrix. $\mathcal{CN}(\boldsymbol{m}, \boldsymbol{R})$ represents the complex Gaussian distribution whose mean is $\boldsymbol{m}$ and covariance matrix is $\boldsymbol{R}$.

II. System Model

As shown in Fig. 1, we consider a hybrid beamforming architecture for a wideband ISAC BS [5]. Assume the BS serves N_{C} communication users while simultaneously detecting some potential targets. To avoid interference among different users, the BS requires at least N_{C} radio frequency (RF) chains to provide data streams. Additionally, N_{S} RF chains are employed to provide sensing services. If $N_{\mathrm{S}} = 0$ indicating the beamforming for target detection completely relies on the communication resource rather than dedicated RF chains. Therefore, the total number of RF chains is

$$N_{\mathrm{RF}} \triangleq N_{\mathrm{C}} + N_{\mathrm{S}}. \tag{1}$$

This work was supported in part by the National Natural Science Foundation of China under Grants U22B2007 and 62071116, and in part by the National Key Research and Development Program of China under Grant 2021YFB2900404. (*Corresponding author: Chenhao Qi*)

Junpeng Guo and Chenhao Qi are with the School of Information Science and Engineering, Southeast University, Nanjing 210096, China (Email: 220240953@seu.edu.cn; qch@seu.edu.cn).

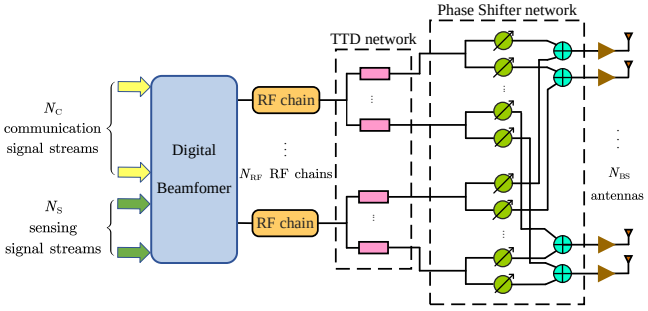

Fig. 1. Illustration of the hybrid beamforming architecture for the BS.

The OFDM modulation is adopted with a center frequency of f_c, a bandwidth of B_w and Q subcarriers. Then we can express the frequency of the qth subcarrier as

$$f_q = f_c + B_w\left(-1 + (2q-1)/Q\right), \tag{2}$$

for $q = 1, 2, \cdots, Q$. We denote $\Omega \triangleq \sin(\omega)$, where $\omega \in (-90°, 90°]$ represents the physical angle. Then the corresponding channel steering vector can be expressed as

$$\boldsymbol{\alpha}(N, \Omega, f_q) = \frac{1}{\sqrt{N}}\left[1, e^{j\pi f_q \Omega}, \cdots, e^{j\pi(N-1) f_q \Omega}\right]^{\mathrm{T}}, \tag{3}$$

where N represents the number of antennas.

The BS is equipped with N_{BS} transmit antennas with half-center-wavelength interval, arranged in a uniform linear array. To handle the angle modulation effects, the TTD network is introduced, where each RF chain is connected to K TTDs and each TTD is sequentially connected to $P = N_{\mathrm{BS}}/K$ phase shifters. Each phase shifter is then connected to the corresponding transmit antenna through a summation network, where the output of the ith phase shifter of all N_{RF} RF chains is summed together and then connected to the ith antenna, for $i = 1, 2, \cdots, N_{\mathrm{BS}}$. According to the properties of the Fourier transform, a TTD with a delay value t introduces a phase shift of $e^{-j2\pi f_q t}$ to the subcarrier with frequency f_q. Let $\boldsymbol{a}_{n,k} \in \mathbb{C}^P$ represent the beamforming vector of the P phase shifters connected by the kth TTD of the nth RF chain, for $k = 1, 2, \cdots, K$ and $n = 1, 2, \cdots, N_{\mathrm{RF}}$. Since the phase shifter can only change the phase of the signal, it must satisfy

$$\left|[\boldsymbol{a}_{n,k}]_p\right| = 1, \tag{4}$$

for $p = 1, 2, \cdots, P$. The phase shifter network is modeled by a matrix $\boldsymbol{A} \in \mathbb{C}^{N_{\mathrm{BS}} \times N_{\mathrm{RF}} K}$ as

$$\boldsymbol{A} \triangleq \frac{1}{\sqrt{N_{\mathrm{BS}}}}\left[\widehat{\boldsymbol{A}}_1, \widehat{\boldsymbol{A}}_2, \cdots, \widehat{\boldsymbol{A}}_{N_{\mathrm{RF}}}\right], \tag{5}$$

where $\widehat{\boldsymbol{A}}_n \triangleq \mathrm{blkdiag}\left\{\boldsymbol{a}_{n,1}, \boldsymbol{a}_{n,2}, \cdots, \boldsymbol{a}_{n,K}\right\}$. The TTD network for the qth subcarrier is modeled by a matrix $\boldsymbol{T}^{(q)} \in \mathbb{C}^{N_{\mathrm{RF}} K \times N_{\mathrm{RF}}}$ as

$$\boldsymbol{T}^{(q)} \triangleq \mathrm{blkdiag}\left\{e^{-j2\pi f_q \boldsymbol{t}_1}, \cdots, e^{-j2\pi f_q \boldsymbol{t}_{N_{\mathrm{RF}}}}\right\}, \tag{6}$$

where $\boldsymbol{t}_n \triangleq [t_{n,1}, t_{n,2}, \cdots, t_{n,K}]^{\mathrm{T}}$ is the vector consisting of the delay values of the K TTDs connected to the nth RF chain. Note that $t_{n,k}$ represents the value of the kth TTD in the nth RF chain, satisfying $t_{n,k} \in [0, t_{\max}]$, where $t_{\max}$ is the maximum delay. Then, the analog beamforming matrix containing the phase shifter network and the TTD network for the qth subcarrier can be expressed as $\boldsymbol{F}_{\mathrm{RF}}^{(q)} \triangleq \boldsymbol{A}\boldsymbol{T}^{(q)}$.

According to the widely used Saleh-Valenzuela channel model in mmWave communications, the channel for the qth subcarrier between the BS and the cth communication user, for $c = 1, 2, \cdots, N_{\mathrm{C}}$, can be expressed as

$$\boldsymbol{h}_c^{(q)} = \sqrt{\frac{N_{\mathrm{BS}}}{L_c}} \sum_{l=1}^{L_c} g_{c,l}^{(q)} \boldsymbol{\alpha}^{\mathrm{H}}\left(N_{\mathrm{BS}}, \Omega_{c,l}^{(q)}, f_q\right), \tag{7}$$

where L_c represents the number of resolvable channel paths. $g_{c,l}^{(q)}$ and $\Omega_{c,l}^{(q)}$ represent the gain and the angle-of-departure of the lth path, for $l = 1, 2, \cdots, L_c$, respectively.

We denote the transmit symbols of the qth subcarrier as $\boldsymbol{s}^{(q)} \in \mathbb{C}^{N_{\mathrm{RF}}}$ satisfying $\mathbb{E}\{\boldsymbol{s}^{(q)}\} = \boldsymbol{0}$ and $\mathbb{E}\{\boldsymbol{s}^{(q)}(\boldsymbol{s}^{(q)})^{\mathrm{H}}\} = \frac{1}{Q}\boldsymbol{I}_{N_{\mathrm{RF}}}$. And we denote the digital beamforming matrix for the qth subcarrier as $\boldsymbol{D}^{(q)} \triangleq \left[\boldsymbol{d}_1^{(q)}, \boldsymbol{d}_2^{(q)}, \cdots, \boldsymbol{d}_{N_{\mathrm{RF}}}^{(q)}\right]$, where $\boldsymbol{d}_n^{(q)} \in \mathbb{C}^{N_{\mathrm{RF}}}$ represents the nth column of $\boldsymbol{D}^{(q)}$. Then the received signal vector $\boldsymbol{y}^{(q)} \triangleq \left[y_1^{(q)}, y_2^{(q)}, \cdots, y_{N_{\mathrm{C}}}^{(q)}\right]^{\mathrm{T}}$ on the qth subcarrier composed by all N_{C} communication users is

$$\boldsymbol{y}^{(q)} = \boldsymbol{H}^{(q)}\boldsymbol{A}\boldsymbol{T}^{(q)}\boldsymbol{D}^{(q)}\boldsymbol{s} + \boldsymbol{\eta}^{(q)}, \tag{8}$$

where $\boldsymbol{H}^{(q)} \triangleq \left[(\boldsymbol{h}_1^{(q)})^{\mathrm{T}}, (\boldsymbol{h}_2^{(q)})^{\mathrm{T}}, \cdots, (\boldsymbol{h}_{N_{\mathrm{C}}}^{(q)})^{\mathrm{T}}\right]^{\mathrm{T}}$ represents the channel matrix between the BS and all communication users, and $\boldsymbol{\eta}^{(q)}$ is the additive white Gaussian noise vector satisfying $\boldsymbol{\eta}^{(q)} \sim \mathcal{CN}\left(\boldsymbol{0}, \sigma^2 \boldsymbol{I}_{N_{\mathrm{C}}}\right)$. Accordingly, the receiving SINR on the qth subcarrier by the cth user is

$$\gamma_c^{(q)} = \frac{\left|\frac{1}{Q}\boldsymbol{h}_n^{(q)}\boldsymbol{A}\boldsymbol{T}^{(q)}\boldsymbol{d}_n^{(q)}\right|^2}{\sum_{i=1, i\neq n}^{N_{\mathrm{RF}}}\left|\frac{1}{Q}\boldsymbol{h}_n^{(q)}\boldsymbol{A}\boldsymbol{T}^{(q)}\boldsymbol{d}_i^{(q)}\right|^2 + \sigma^2}, \tag{9}$$

where σ^2 is the power of the additive white Gaussian noise. The SINR requirement of the qth subcarrier by the cth communication user is denoted as $\Gamma_c^{(q)}$. Then we require $\gamma_c^{(q)} \geqslant \Gamma_c^{(q)}$, for $q = 1, 2, \cdots, Q$ and $c = 1, 2, \cdots, N_{\mathrm{C}}$. For the sensing functionality of the BS, we need to generate beams to cover all possible directions of potential targets [6]. Suppose the space is sampled by M points, and let the azimuth angle of the mth sampling point be $\Phi_m \in (-1, 1]$, for $m = 1, 2, \cdots, M$. Then, the spatial sampling matrix for the qth subcarrier can be expressed as

$$\boldsymbol{\Phi}^{(q)} = \sqrt{N_{\mathrm{BS}}}\left[\boldsymbol{\alpha}(N_{\mathrm{BS}}, \Phi_1, f_q), \cdots, \boldsymbol{\alpha}(N_{\mathrm{BS}}, \Phi_M, f_q)\right]^{\mathrm{H}}. \tag{10}$$

We aim at approaching a predefined sensing beam pattern $\boldsymbol{b} \in \mathbb{R}^M$, which requires the BS to generate additional sensing beams with the same RF chain originally generating the communication beam. The beam pattern of the transmit signal of the BS can be viewed as the sum of the beam patterns across all subcarriers, where the qth beam pattern can be expressed as $\left|\frac{1}{Q}\boldsymbol{\Phi}^{(q)}\sum_{n=1}^{N_{\mathrm{RF}}}\boldsymbol{A}\boldsymbol{T}^{(q)}\boldsymbol{d}_n^{(q)}\right|$. The constraints include the SINR requirements of the communication users and the maximum transmit power of the BS. Such a problem in terms of the digital beamformer, the true-time-delayer network and the phase shifter network can be expressed as

$$\min_{\boldsymbol{A}, \boldsymbol{T}^{(q)}, \boldsymbol{D}^{(q)}} \left\|\sum_{q=1}^{Q}\left|\frac{1}{Q}\boldsymbol{\Phi}^{(q)}\sum_{n=1}^{N_{\mathrm{RF}}}\boldsymbol{A}\boldsymbol{T}^{(q)}\boldsymbol{d}_n^{(q)}\right| - \boldsymbol{b}\right\|_2 \tag{11a}$$

$$\text{s.t.} \quad \left\|\boldsymbol{A}\boldsymbol{T}^{(q)}\boldsymbol{D}^{(q)}\right\|_{\mathrm{F}}^2 \leqslant P_{\mathrm{T}}, q = 1, 2, \cdots, Q, \tag{11b}$$

$$\gamma_c^{(q)} \geqslant \Gamma_c^{(q)}, q = 1, 2, \cdots, Q, c = 1, 2, \cdots, N_{\mathrm{C}}, \tag{11c}$$

where P_{T} represents the maximum transmit power of the BS, and $\boldsymbol{B} \triangleq \mathrm{diag}\{\boldsymbol{b}\}$ is a diagonal matrix.

III. Hybrid Beamforming Design

Due to the strong coupling among the design variables, (11) is difficult to handle. Therefore, we adopt the ADMM framework to decompose this problem. To decouple $\boldsymbol{A}$, $\boldsymbol{T}^{(q)}$ and $\boldsymbol{D}^{(q)}$ in (11b), we introduce an auxiliary variable $\boldsymbol{U}^{(q)}$ [7]. We denote the sensing beam pattern of the qth subcarrier as $\boldsymbol{b}^{(q)}$ satisfying $\sum_{q=1}^{Q}\boldsymbol{b}^{(q)}=\boldsymbol{b}$. Then we can distribute the sensing beam pattern among different subcarriers for optimization. To improve the design flexibility, we introduce a phase vectors $\boldsymbol{p}^{(q)}$ to convert the modulus summation into a linear summation. By denoting $\boldsymbol{U}^{(q)}\triangleq\boldsymbol{A}\boldsymbol{T}^{(q)}\boldsymbol{D}^{(q)}$, (11) can be rewritten as

$$\min_{\substack{\boldsymbol{A},\boldsymbol{T}^{(q)},\boldsymbol{D}^{(q)},\\ \boldsymbol{B}^{(q)},\boldsymbol{p}^{(q)}}} \left\|\sum_{q=1}^{Q}\left(\frac{1}{Q}\boldsymbol{\Phi}^{(q)}\sum_{n=1}^{N_{\mathrm{RF}}}\boldsymbol{u}_n^{(q)}-\boldsymbol{B}^{(q)}\boldsymbol{p}^{(q)}\right)\right\|_2 \tag{12a}$$

$$\text{s.t.}\quad \boldsymbol{U}^{(q)}=\boldsymbol{A}\boldsymbol{T}^{(q)}\boldsymbol{D}^{(q)}, \tag{12b}$$

$$\left\|\boldsymbol{U}^{(q)}\right\|_{\mathrm{F}}^2\leqslant P_{\mathrm{T}}\text{ and (11c)}, \tag{12c}$$

where $\boldsymbol{u}_n^{(q)}$ represents the nth column of $\boldsymbol{U}^{(q)}$, and $\boldsymbol{B}^{(q)}\triangleq\mathrm{diag}\{\boldsymbol{b}^{(q)}\}$ is a diagonal matrix. By incorporating (12b) as an augmented Lagrange term to the objective function, we have

$$\mathcal{L}=\left\|\sum_{q=1}^{Q}\left(\frac{1}{Q}\boldsymbol{\Phi}^{(q)}\sum_{n=1}^{N_{\mathrm{RF}}}\boldsymbol{u}_n^{(q)}-\boldsymbol{B}^{(q)}\boldsymbol{p}^{(q)}\right)\right\|_2+\frac{\alpha}{2}\sum_{q=1}^{Q}\left\|\boldsymbol{U}^{(q)}+\frac{\boldsymbol{\Lambda}^{(q)}}{\alpha}-\boldsymbol{A}\boldsymbol{T}^{(q)}\boldsymbol{D}^{(q)}\right\|_{\mathrm{F}}^2, \tag{13}$$

where α and $\boldsymbol{\Lambda}^{(q)}$ represent the penalty parameter and the dual variable introduced in the ADMM framework, respectively. To simplify the representation, we define

$$\boldsymbol{S}_{\mathrm{n}}\triangleq[\boldsymbol{I}_{N_{\mathrm{BS}}},\cdots,\boldsymbol{I}_{N_{\mathrm{BS}}}]\in\mathbb{R}^{N_{\mathrm{BS}}\times N_{\mathrm{RF}}N_{\mathrm{BS}}}. \tag{14}$$

We stack $\boldsymbol{u}_1^{(q)},\boldsymbol{u}_2^{(q)},\cdots,\boldsymbol{u}_{N_{\mathrm{RF}}}^{(q)}$ together and define

$$\boldsymbol{u}^{(q)}\triangleq\left[(\boldsymbol{u}_1^{(q)})^{\mathrm{T}},(\boldsymbol{u}_2^{(q)})^{\mathrm{T}},\cdots,(\boldsymbol{u}_{N_{\mathrm{RF}}}^{(q)})^{\mathrm{T}}\right]^{\mathrm{T}}. \tag{15}$$

Then, the beam pattern for the qth subcarrier can be represented as $\sum_{i=1}^{N_{\mathrm{RF}}}\boldsymbol{u}_n^{(q)}=\boldsymbol{S}_{\mathrm{n}}\boldsymbol{u}^{(q)}$. In fact, the first term on the right hand of the equation of (13) can be rewritten as $\left\|\boldsymbol{S}_{\mathrm{Q}}\left(\frac{1}{Q}\boldsymbol{\Phi}_{\mathrm{Q}}\boldsymbol{S}_{\mathrm{R}}\boldsymbol{u}-\boldsymbol{B}_{\mathrm{Q}}\boldsymbol{p}_{\mathrm{Q}}\right)\right\|_2$, where

$$\boldsymbol{S}_{\mathrm{Q}}\triangleq[\boldsymbol{I}_M,\boldsymbol{I}_M,\cdots,\boldsymbol{I}_M]\in\mathbb{R}^{M\times QM}, \tag{16}$$

$$\boldsymbol{u}\triangleq\left[(\boldsymbol{u}^{(1)})^{\mathrm{T}},(\boldsymbol{u}^{(2)})^{\mathrm{T}},\cdots,(\boldsymbol{u}^{(Q)})^{\mathrm{T}}\right]^{\mathrm{T}}\in\mathbb{C}^{QN_{\mathrm{RF}}N_{\mathrm{BS}}}, \tag{17}$$

$$\boldsymbol{p}_{\mathrm{Q}}\triangleq\left[(\boldsymbol{p}^{(1)})^{\mathrm{T}},(\boldsymbol{p}^{(2)})^{\mathrm{T}},\cdots,(\boldsymbol{p}^{(Q)})^{\mathrm{T}}\right]^{\mathrm{T}}\in\mathbb{C}^{QM}, \tag{18}$$

$$\boldsymbol{\Phi}_{\mathrm{Q}}\triangleq\mathrm{blkdiag}\left\{\boldsymbol{\Phi}^{(1)},\boldsymbol{\Phi}^{(2)},\cdots,\boldsymbol{\Phi}^{(Q)}\right\}\in\mathbb{C}^{QM\times QN_{\mathrm{BS}}}, \tag{19}$$

$$\boldsymbol{S}_{\mathrm{R}}\triangleq\mathrm{blkdiag}\left\{\boldsymbol{S}_{\mathrm{n}},\boldsymbol{S}_{\mathrm{n}},\cdots,\boldsymbol{S}_{\mathrm{n}}\right\}\in\mathbb{R}^{QN_{\mathrm{BS}}\times QN_{\mathrm{RF}}N_{\mathrm{BS}}}, \tag{20}$$

$$\boldsymbol{B}_{\mathrm{Q}}\triangleq\mathrm{blkdiag}\left\{\boldsymbol{B}^{(1)},\boldsymbol{B}^{(2)},\cdots,\boldsymbol{B}^{(Q)}\right\}\in\mathbb{R}^{QM\times QM} \tag{21}$$

represent vectors or matrices by stacking the existing symbols together. Then, (11) is finally transformed into

$$\min_{\substack{\boldsymbol{U}^{(q)},\boldsymbol{A},\boldsymbol{T}^{(q)},\boldsymbol{D}^{(q)},\\ \boldsymbol{B}^{(q)},\boldsymbol{p}^{(q)},\boldsymbol{\Lambda}^{(q)}}} \left\|\boldsymbol{S}_{\mathrm{Q}}\left(\frac{1}{Q}\boldsymbol{\Phi}_{\mathrm{Q}}\boldsymbol{S}_{\mathrm{R}}\boldsymbol{u}-\boldsymbol{B}_{\mathrm{Q}}\boldsymbol{p}_{\mathrm{Q}}\right)\right\|_2+\frac{\alpha}{2}\sum_{q=1}^{Q}\left\|\boldsymbol{U}^{(q)}+\frac{\boldsymbol{\Lambda}^{(q)}}{\alpha}-\boldsymbol{A}\boldsymbol{T}^{(q)}\boldsymbol{D}^{(q)}\right\|_{\mathrm{F}}^2 \tag{22a}$$

$$\text{s.t.}\quad \left\|\boldsymbol{U}^{(q)}\right\|_{\mathrm{F}}^2\leqslant P_{\mathrm{T}}\text{ and (11c)}. \tag{22b}$$

Note that (22) can be decomposed into multiple manageable subproblems, which can be solved alternately and iteratively. In the following, we will propose a TTDHBF scheme to optimize $\boldsymbol{U}^{(q)}$, $\boldsymbol{A}$, $\boldsymbol{T}^{(q)}$, $\boldsymbol{D}^{(q)}$, $\boldsymbol{B}^{(q)}$, $\boldsymbol{p}^{(q)}$ and $\boldsymbol{\Lambda}^{(q)}$.

A. Optimization of the auxiliary variable

With the other variables fixed, the optimization problem for $\boldsymbol{U}^{(q)}$ can be expressed as

$$\min_{\boldsymbol{U}^{(q)}} \left\|\boldsymbol{S}_{\mathrm{Q}}\left(\frac{1}{Q}\boldsymbol{\Phi}_{\mathrm{Q}}\boldsymbol{S}_{\mathrm{R}}\boldsymbol{u}-\boldsymbol{B}_{\mathrm{Q}}\boldsymbol{p}_{\mathrm{Q}}\right)\right\|_2+\frac{\alpha}{2}\sum_{q=1}^{Q}\left\|\boldsymbol{U}^{(q)}+\frac{\boldsymbol{\Lambda}^{(q)}}{\alpha}-\boldsymbol{A}\boldsymbol{T}^{(q)}\boldsymbol{D}^{(q)}\right\|_{\mathrm{F}}^2 \tag{23a}$$

$$\text{s.t.}\quad \left\|\boldsymbol{U}^{(q)}\right\|_{\mathrm{F}}^2\leqslant P_{\mathrm{T}},q=1,2,\cdots,Q, \tag{23b}$$

$$\gamma_c^{(q)}\geqslant\Gamma_c^{(q)},q=1,2,\cdots,Q,c=1,2,\cdots,N_{\mathrm{C}}, \tag{23c}$$

In fact, this problem can be easily converted into a second-order cone programming problem [8], which can be readily solved by existing optimization toolboxes.

B. Optimization of the beam pattern

With the other variables fixed, the optimization problem for $\boldsymbol{B}^{(q)}$ can be expressed as

$$\min_{\boldsymbol{B}^{(q)}} \left\|\boldsymbol{S}_{\mathrm{Q}}\left(\frac{1}{Q}\boldsymbol{\Phi}_{\mathrm{Q}}\boldsymbol{S}_{\mathrm{R}}\boldsymbol{u}-\boldsymbol{B}_{\mathrm{Q}}\boldsymbol{p}_{\mathrm{Q}}\right)\right\|_2 \tag{24a}$$

$$\text{s.t.}\ \sum\nolimits_{q=1}^{Q}\boldsymbol{B}^{(q)}=\boldsymbol{B}, \tag{24b}$$

which is a typical convex optimization problem and can be conveniently solved using existing optimization toolboxes.

C. Optimization of the phase

With the other variables fixed, the optimization problem for $\boldsymbol{p}^{(q)}$ can be expressed as

$$\min_{\boldsymbol{p}^{(q)}} \left\|\boldsymbol{S}_{\mathrm{Q}}\left(\frac{1}{Q}\boldsymbol{\Phi}_{\mathrm{Q}}\boldsymbol{S}_{\mathrm{R}}\boldsymbol{u}-\boldsymbol{B}_{\mathrm{Q}}\boldsymbol{p}_{\mathrm{Q}}\right)\right\|_2 \tag{25a}$$

$$\text{s.t.}\ \left|\left[\boldsymbol{p}^{(q)}\right]_m\right|=1,m=1,2,\cdots,M, \tag{25b}$$

which is a constrained least squares (LS) problem. Without (25b), the solution to this problem is given by

$$\widehat{\boldsymbol{p}}_{\mathrm{Q}}=\left(\boldsymbol{B}_{\mathrm{Q}}^{\mathrm{H}}\boldsymbol{S}_{\mathrm{Q}}^{\mathrm{H}}\boldsymbol{S}_{\mathrm{Q}}\boldsymbol{B}_{\mathrm{Q}}\right)^{-1}\boldsymbol{B}_{\mathrm{Q}}^{\mathrm{H}}\boldsymbol{S}_{\mathrm{Q}}^{\mathrm{H}}\boldsymbol{S}_{\mathrm{Q}}\boldsymbol{\Phi}_{\mathrm{Q}}\boldsymbol{S}_{\mathrm{R}}\boldsymbol{u}. \tag{26}$$

Considering (25b), the final solution to (25) is given by

$$\left[\boldsymbol{p}_{\mathrm{Q}}\right]_v=\frac{[\widehat{\boldsymbol{p}}_{\mathrm{Q}}]_v}{|[\widehat{\boldsymbol{p}}_{\mathrm{Q}}]_v|},v=1,2,\cdots,QM. \tag{27}$$

D. Optimization of the phase shifter network

With the other variables fixed, the optimization problem for $\boldsymbol{A}$ can be expressed as

$$\min_{\boldsymbol{A}} \sum_{q=1}^{Q}\left\|\boldsymbol{U}^{(q)}+\frac{\boldsymbol{\Lambda}^{(q)}}{\alpha}-\boldsymbol{A}\boldsymbol{T}^{(q)}\boldsymbol{D}^{(q)}\right\|_{\mathrm{F}}^2. \tag{28}$$

In fact, we can decompose (28) into $N_{\mathrm{RF}}\times K$ subproblems [5], where the (n,k)th subproblem can be expressed as

$$\max_{\boldsymbol{a}_{n,k}} \sum_{q=1}^{Q}\mathrm{Re}\left\{(\boldsymbol{r}_{n,k}^{(q)})^{\mathrm{H}}\boldsymbol{a}_{n,k}e^{-j2\pi f_q t_{n,k}}\right\} \tag{29a}$$

$$\text{s.t.}\ \left|[\boldsymbol{a}_{n,k}]_p\right|=1,p=1,2,\cdots,P, \tag{29b}$$

with $\boldsymbol{r}_{n,k}^{(q)}\triangleq\left[(\boldsymbol{U}^{(q)}+\frac{\boldsymbol{\Lambda}^{(q)}}{\alpha})(\boldsymbol{D}^{(q)})^{\dagger}\right]_{P(k-1)+1:Pk,n}\in\mathbb{C}^P$.

The solution to this problem is given by

$$\boldsymbol{a}_{n,k} = \exp\left(j\angle\left(\sum\nolimits_{q=1}^{Q} \boldsymbol{r}_{n,k}^{(q)} e^{j2\pi f_q t_{n,k}}\right)\right). \tag{30}$$

Then, $\boldsymbol{A}$ can be obtained based on (30) and (5).

E. Optimization of the TTD network

With the other variables fixed, the optimization problem for $\boldsymbol{T}^{(q)}$ can be expressed as

$$\min_{\boldsymbol{T}^{(q)}} \sum_{q=1}^{Q} \left\| \boldsymbol{U}^{(q)} + \frac{\boldsymbol{\Lambda}^{(q)}}{\alpha} - \boldsymbol{A}\boldsymbol{T}^{(q)}\boldsymbol{D}^{(q)} \right\|_{\mathrm{F}}^{2}. \tag{31}$$

Similar to the optimization of the phase shifter network, (31) can also be decomposed into $N_{\mathrm{RF}} \times K$ subproblems [5], where the (n,k)th subproblem can be expressed as

$$\max_{t_{n,k}} \sum_{q=1}^{Q} \mathrm{Re}\left\{ (\boldsymbol{r}_{n,k}^{(q)})^{\mathrm{H}} \boldsymbol{a}_{n,k} e^{-j2\pi f_q t_{n,k}} \right\} \tag{32a}$$

$$\text{s.t. } t_{n,k} \in [0, t_{\max}]. \tag{32b}$$

Although this problem is highly non-convex, an effective suboptimal solution can be obtained using a one-dimensional search method. Assume the delay values are taken within $\mathcal{T} = \left\{0, \frac{t_{\max}}{T-1}, \frac{2t_{\max}}{T-1}, \cdots, t_{\max}\right\}$ with T sampling points. The final solution to this problem can be expressed as

$$t_{n,k} = \arg\max_{t \in \mathcal{T}} \sum_{q=1}^{Q} \mathrm{Re}\left\{ (\boldsymbol{r}_{n,k}^{(q)})^{\mathrm{H}} \boldsymbol{a}_{n,k} e^{-j2\pi f_q t} \right\}. \tag{33}$$

Then, $\boldsymbol{T}^{(q)}$ can be obtained based on (33) and (6).

F. Optimization of the digital beamformer

With the other variables fixed, the optimization problem for $\boldsymbol{D}^{(q)}$ can be expressed as

$$\min_{\boldsymbol{D}^{(q)}} \sum_{q=1}^{Q} \left\| \boldsymbol{U}^{(q)} + \frac{\boldsymbol{\Lambda}^{(q)}}{\alpha} - \boldsymbol{A}\boldsymbol{T}^{(q)}\boldsymbol{D}^{(q)} \right\|_{\mathrm{F}}^{2}. \tag{34}$$

This is a LS problem with the solution expressed as

$$\boldsymbol{D}^{(q)} = \left((\boldsymbol{T}^{(q)})^{\mathrm{H}} \boldsymbol{A}^{\mathrm{H}} \boldsymbol{A} \boldsymbol{T}^{(q)}\right)^{-1} (\boldsymbol{T}^{(q)})^{\mathrm{H}} \boldsymbol{A}^{\mathrm{H}} \left(\boldsymbol{U}^{(q)} + \frac{\boldsymbol{\Lambda}^{(q)}}{\alpha}\right). \tag{35}$$

G. Optimization of the dual variable

According to the ADMM framework [9], the optimization expression for $\boldsymbol{\Lambda}^{(q)}$ in the zth iteration is given by

$$\boldsymbol{\Lambda}_{z}^{(q)} = \boldsymbol{\Lambda}_{z-1}^{(q)} + \alpha\left(\boldsymbol{U}^{(q)} - \boldsymbol{A}\boldsymbol{T}^{(q)}\boldsymbol{D}^{(q)}\right). \tag{36}$$

H. Update of α

Owing to the incorporation of Lagrange multipliers within the ADMM framework, it is necessary to keep α non-regressive throughout the iterations [7]. Therefore, as the number of iterations increases, $\boldsymbol{A}\boldsymbol{T}^{(q)}\boldsymbol{D}^{(q)}$ gradually approaches $\boldsymbol{U}^{(q)}$. We update α at the zth iteration by

$$\alpha_z = \begin{cases} \lambda_1 \alpha_{z-1}, G_1 \geqslant \mu_1 G_2, \\ \alpha_{z-1}, \text{otherwise}, \end{cases} \tag{37}$$

where G_1 and G_2 represent the first and second term in (13), respectively. The variables and the parameter are alternately updated in each iteration, and the iterations are performed until a predefined number of iterations $Z_{\max}$ is reached. The complete procedure of the proposed TTDHBF scheme is summarized in **Algorithm 1**.

Algorithm 1 TTDHBF scheme for wideband ISAC

Input: $\boldsymbol{H}^{(q)}, \boldsymbol{\Phi}_{\mathrm{Q}}, \boldsymbol{b}, P_T, \Gamma_1, \Gamma_2, \cdots, \Gamma_{N_{\mathrm{C}}}$ and σ^2.
Initialize $\boldsymbol{U}^{(q)}, \boldsymbol{A}, \boldsymbol{T}^{(q)}, \boldsymbol{D}^{(q)}, \boldsymbol{B}^{(q)}, \boldsymbol{p}^{(q)}, \boldsymbol{\Lambda}$ and α.
Set $z \leftarrow 1$.
while $z \leqslant Z_{\max}$ **do**
  Obtain $\boldsymbol{U}^{(q)}$ by solving (23).
  Obtain $\boldsymbol{B}^{(q)}$ by solving (24).
  Obtain $\boldsymbol{p}^{(q)}$ via (26) and (27).
  Obtain $\boldsymbol{A}$ via (30) and (5).
  Obtain $\boldsymbol{T}^{(q)}$ via (33) and (6).
  Obtain $\boldsymbol{D}^{(q)}$ via (35).
  Obtain $\boldsymbol{\Lambda}^{(q)}$ via (36).
  Update α according to (37).
  $z \leftarrow z + 1$.
end while
Output: $\boldsymbol{A}, \boldsymbol{T}^{(q)}$ and $\boldsymbol{D}^{(q)}$.

Now we evaluate the computational complexity of the proposed TTFHBF scheme. The TTDHBF scheme undergoes $Z_{\max}$ iterations, where each iteration contains eight subproblems. Since we provide closed-form expressions for most variables, the computational complexity mainly comes from updating $\boldsymbol{U}^{(q)}$, $\boldsymbol{B}^{(q)}$ and $\boldsymbol{T}^{(q)}$. Note that we use CVX to solve (23) and (24), with the corresponding computational complexity being respectively $\mathcal{O}\big(\left(N_{\mathrm{BS}}N_{\mathrm{RF}}Q\right)^{3.5}\log_2\left(1/\varepsilon_1\right)\big)$ and $\mathcal{O}\big(\left(MQ\right)^{3.5}\log_2\left(1/\varepsilon_2\right)\big)$, where ε_1 and ε_2 represent the the solution accuracy used for solving (23) and (24), respectively. Additionally, the computational complexity for solving (33) is $\mathcal{O}\big(TQPN_{\mathrm{BS}}N_{\mathrm{RF}}^2\big)$. In total, the computational complexity of the proposed TTDHBF algorithm is

$$\mathcal{O}\Big(Z_{\max}\big(\left(N_{\mathrm{BS}}N_{\mathrm{RF}}Q\right)^{3.5}\log_2(1/\varepsilon_1) + \left(MQ\right)^{3.5}\log_2(1/\varepsilon_2) + TQPN_{\mathrm{BS}}N_{\mathrm{RF}}^2\big)\Big). \tag{38}$$

IV. Simulation Results

We consider a wideband ISAC BS equipped with $N_{\mathrm{BS}} = 64$ transmit antennas, $N_{\mathrm{C}} = 3$ communication RF chains and $N_{\mathrm{S}} = 0$ sensing RF chain, implying that the sensing function entirely relies on communication resources instead of dedicated sensing RF chains. Each RF chain connects to $K = 8$ TTDs, and each TTD connects to $P = 8$ antennas. The center frequency of the transmit signal is $f_c = 100\mathrm{GHz}$, with a bandwidth of $B_w = 20\mathrm{GHz}$ and $Q = 10$ subcarriers [5]. The BS transmits with a power of $P_{\mathrm{T}} = 20\mathrm{dBm}$, and the noise power is $\sigma^2 = 0\mathrm{dBm}$. The BS simultaneously serves $N_{\mathrm{C}} = 3$ communication users, located at -40°, -15° and 10° with SINR requirement of $\Gamma = 5\mathrm{dB}$ for each subcarrier of each user, respectively. There is one line-of-sight path with the channel gain obeying $\mathcal{CN}(0,1)$ and one non-line-of-sight path with the channel gain obeying $\mathcal{CN}(0,0.01)$ between the BS and each user. The BS samples the space within $(-90^\circ, 90^\circ]$ using $M = 360$ points, and the sensing area is $[45^\circ, 50^\circ]$. According to the law of energy conservation, the sensing beam gain within this area is

$$\sqrt{\frac{2N_{\mathrm{RF}}P_{\mathrm{T}}}{\sin(50^\circ) - \sin(45^\circ)}}. \tag{39}$$

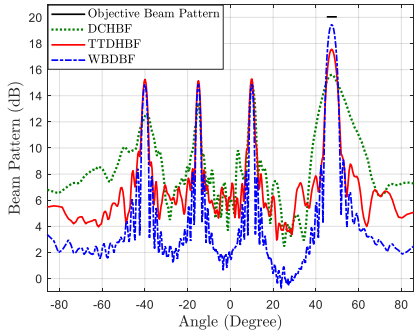

Fig. 2. Comparisons of beam patterns for different schemes.

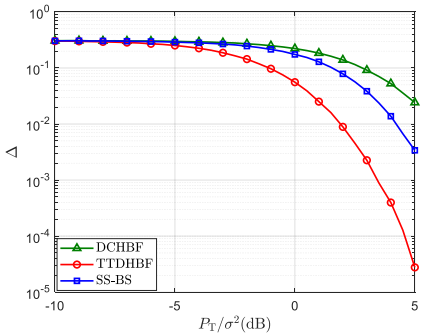

Fig. 3. NMSE comparisons of distance estimation for different schemes.

We set $\lambda_1 = 1.25$ and $\mu_1 = 1$ to update α.

As shown in Fig. 2, we compare the beam patterns of the transmit signal of the BS, using the digitally compensated hybrid beamforming (DCHBF) [2], the wideband fully-digital beamforming (WBDBF) and the proposed TTDHBF schemes. Due to limited design flexibility, DCHBF struggles to simultaneously align beams in both communication and sensing directions, leading to an overall beam broadening, which is particularly pronounced in regions with larger angles, where the beam squint effect becomes more significant. The proposed TTDHBF scheme can approach the performance of WBDBF much better than DCHBF, and therefore can effectively eliminate the beam squint effect under the hybrid beamforming architecture.

To evaluate the sensing performance of the TTDHBF scheme, we compare it with the DCHBF scheme and the beam squint (SS-BS) scheme [4] in terms of the normalized mean squared error (NMSE) of distance estimation of a target. The NMSE is defined as $\Delta \triangleq (d - \hat{d})^2/d^2$, where d and $\hat{d}$ represent the actual distance and the estimated distance of the target, respectively. The distance estimation of the target is jointly performed by all the subcarriers using their measurements [10]. We suppose that the sensing beam designed by these three schemes all covers the target. From Fig. 3, it is seen that the TTDHBF scheme outperforms the other two schemes. The reason is provided as follows. For the SS-BS scheme, due to the beam misalignment caused by the beam squint in wideband mmWave system, it is difficult for all subcarriers to provide effective beam gain for target sensing, which reduces the number of subcarriers valid for distance estimation of the target. For the DCHBF scheme, the beam gain of the sensing beam is smaller than that of the TTDHBF scheme, which can also be observed from Fig. 2.

In Fig. 4, we provide the trade-off between the communication and sensing performance of the ISAC system under different antenna configurations for the TTDHBF scheme. We define the sensing NMSE as $\Upsilon \triangleq \|\frac{1}{Q}\boldsymbol{S}_{\mathrm{Q}}\boldsymbol{\Phi}_{\mathrm{Q}}\boldsymbol{S}_{\mathrm{R}}\boldsymbol{u} - \boldsymbol{b}\|_2^2 / \|\boldsymbol{b}\|_2^2$. It is seen that higher SINR requirement leads to worse performance of the sensing NMSE. Besides, as the number of BS antennas increases, the sensing NMSE performance also improves, because a larger antenna array can generate narrower beams and achieve better resource allocation.

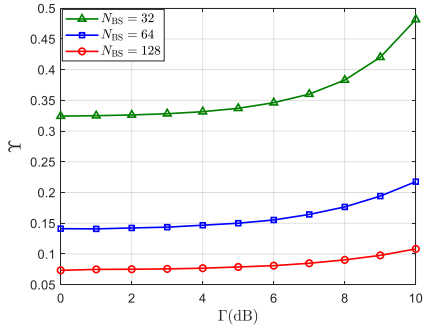

Fig. 4. Trade-off between communication and sensing performance.

V. Conclusion

In this letter, we have proposed a TTDHBF scheme for wideband mmWave MIMO ISAC. We aim at making the sum of beam patterns across all subcarriers approach a predefined sensing beam pattern, subject to the constraints of the SINR requirements of communication users and the maximum transmit power of the BS. Simulation results have demonstrated that the proposed scheme outperforms existing wideband hybrid beamforming schemes. For future work, we will continue to explore low-complexity algorithms for wideband hybrid beamforming design.

References

[1] C. Qi, W. Ci, J. Zhang, and X. You, "Hybrid beamforming for millimeter wave MIMO integrated sensing and communications," *IEEE Commun. Lett.*, vol. 26, no. 5, pp. 1136–1140, May 2022.

[2] A. M. Elbir, K. V. Mishra, and S. Chatzinotas, "Terahertz-band joint ultra-massive MIMO radar-communications: Model-based and model-free hybrid beamforming," *IEEE J. Sel. Topics Signal Process.*, vol. 15, no. 6, pp. 1468–1483, Nov. 2021.

[3] L. Dai, J. Tan, Z. Chen, and H. V. Poor, "Delay-phase precoding for wideband THz massive MIMO," *IEEE Trans. Wireless Commun.*, vol. 21, no. 9, pp. 7271–7286, Sep. 2022.

[4] F. Gao, L. Xu, and S. Ma, "Integrated sensing and communications with joint beam-squint and beam-split for mmWave/THz massive MIMO," *IEEE Trans. Commun.*, vol. 71, no. 5, pp. 2963–2976, May 2023.

[5] Z. Wang, X. Mu, Y. Liu, and R. Schober, "TTD configurations for near-field beamforming: Parallel, serial, or hybrid?" *IEEE Trans. Commun.*, vol. 72, no. 6, pp. 3783–3799, June 2024.

[6] Z. Cheng and B. Liao, "Qos-aware hybrid beamforming and DOA estimation in multi-carrier dual-function radar-communication systems," *IEEE J. Sel. Areas Commun.*, vol. 40, no. 6, pp. 1890–1905, June 2022.

[7] B. Wang, L. Wu, Z. Cheng, and Z. He, "Exploiting constructive interference in symbol level hybrid beamforming for dual-function radar-communication system," *IEEE Wireless Commun. Lett.*, vol. 11, no. 10, pp. 2071–2075, Oct. 2022.

[8] Z. Q. Luo and W. Yu, "An introduction to convex optimization for communications and signal processing," *IEEE J. Sel. Areas Commun.*, vol. 24, no. 8, pp. 1426–1438, Aug. 2006.

[9] S. Boyd *et al.*, "Distributed optimization and statistical learning via the alternating direction method of multipliers," *Found. Trends Mach. Learn.*, vol. 3, no. 1, pp. 1–122, Feb. 2011.

[10] R. Zhang and et al., "Channel training-aided target sensing for terahertz integrated sensing and massive MIMO communications," *IEEE Internet of Things J., early access*, pp. 1–1, 2024.